PAPER

A comparison of the magnetism of cobalt-, manganese-, and nickel-ferrite nanoparticles

To cite this article: Ç E Demirci *et al* 2018 *J. Phys. D: Appl. Phys.* **51** 025003

IOP Publishing Journal of Physics D: Applied Physics

J. Phys. D: Appl. Phys. **51** (2018) 025003 (10pp) https://doi.org/10.1088/1361-6463/aa9d79

A comparison of the magnetism of cobalt-, manganese-, and nickel-ferrite nanoparticles

Ç E Demirci[1,2], P K Manna[2], Y Wroczynskyj[2], S Aktürk[1] and J van Lierop[2,3]

[1] Department of Physics, Muğla Sıtkı Koçman University, 48000, Muğla, Turkey
[2] Department of Physics and Astronomy, University of Manitoba, Winnipeg, MB, R3T 2N2, Canada
[3] Manitoba Institute for Materials, Winnipeg, MB, R3T 2N2, Canada

E-mail: elifdemirci@mu.edu.tr and Johan.van.Lierop@umanitoba.ca

Received 9 August 2017, revised 20 November 2017
Accepted for publication 27 November 2017
Published 19 December 2017

Abstract

The microstructure, composition and magnetism of $CoFe_2O_4$, $MnFe_2O_4$ and $NiFe_2O_4$ nanoparticles of comparable sizes (~20 nm) and interparticle spacings (~20 nm) have been characterized from 10 to 400 K. The cation distributions of the tetrahedral and octahedral sites of the particles, that have cubic spinel structures, have a high degree of inversion, ~0.98 for $CoFe_2O_4$, ~0.80 for $MnFe_2O_4$ and $NiFe_2O_4$ nanoparticles. The blocking temperatures were ~300 K for the $MnFe_2O_4$ and $NiFe_2O_4$ nanoparticles, while the $CoFe_2O_4$ nanoparticles, due to their higher intrinsic anisotropy had a significantly higher blocking temperature above 400 K. Specifically, the magnetocrystalline anisotropy of the $CoFe_2O_4$ nanoparticles was $K = (2.96 \pm 0.03) \times 10^6$ ergs cm^{-3}, while for the $MnFe_2O_4$ nanoparticles, $K = (0.04 \pm 0.01) \times 10^6$ ergs cm^{-3}, and for the $NiFe_2O_4$ nanoparticles, $K = (0.07 \pm 0.01) \times 10^6$ ergs cm^{-3}. The magnetism of these three ferrite systems are discussed in detail with regards to their microstructures and cation distributions.

Keywords: cobalt ferrite, manganese ferrite, nickel ferrite, cation distribution

(Some figures may appear in colour only in the online journal)

1. Introduction

Nanoparticles of spinel ferrites are one of the most attractive materials for the development of new technologies due to their behaviour at the nanoscale. A large number of ferrimagnetic compounds with spinel structures have found a wide range of applications, such as in spintronics [1], magnetocaloric refrigeration [2, 3] magnetic resonance imaging [4] and magnetic hyperthermia [5]. A thorough understanding of their magnetic properties allows us to realize new potential applications with tailored properties that can be achieved with decreasing particle size, changing the cation distributions of the tetrahedral and octahedral sites, or substituting these sites with different ions, such as the rare-earths to further alter the magnetism for applications.

The ideal spinel structure has a face centered cubic unit cell with 32 O^{2-} anions and metal ions situated in the possible interstitial sites between the oxygen ions [6]. The general structural formula of a spinel can be represented as $(M_{1-x}Fe_x)[M_xFe_{2-x}]O_4$ (M is the metal ion) [7], where round and square brackets denote the tetrahedral (A site) and octahedral (B site) coordinations and x is the inversion parameter which is a quantity identifying the fraction of divalent ions in octahedral sites. The spinel structure is called 'normal' if all the divalent ions are located in tetrahedral sites, $(M^{2+})^{tet}(Fe^{3+})^{oct}O_4$ and $x = 0$, 'inverse' if all the divalent ions are located in octahedral sites, $(Fe^{3+})^{tet}(M^{2+}Fe^{3+})^{oct}O_4$ and $x = 1$ [6]. If the divalent ions are located on both tetrahedral and octahedral sites ($0 < x < 1$), the spinel is partially inverted [8]. The inversion degree may depend on the synthesis method [9–11],

thermal history of the materials (due to annealing) [10, 12], and particle size effects [13].

$CoFe_2O_4$, $MnFe_2O_4$ and $NiFe_2O_4$ are spinels where the distribution of the cations among the tetrahedral and octahedral sites can be quite different [8] resulting in quite different magnetism, especially at the nanoscale. For example, partially inverted spinel structures for $CoFe_2O_4$ and $MnFe_2O_4$ were reported in which 80% Co^{2+} [8] and 20% Mn^{2+} [14] ions are in octahedral sites with high and low degree of inversion for $CoFe_2O_4$ [15] and $MnFe_2O_4$ [8], respectively. $MnFe_2O_4$ is a more complex system compared to $CoFe_2O_4$ and $NiFe_2O_4$, as it can have different oxidation states of Mn atoms (Mn^{2+} and/or Mn^{3+}) [16–18]. By contrast, $NiFe_2O_4$ is a totally inverted spinel structure in which all the nickel ions are located in octahedral sites [17].

In this paper, we present the structural, compositional and magnetic properties of $CoFe_2O_4$, $MnFe_2O_4$ and $NiFe_2O_4$ nanoparticles with similar sizes (∼20 nm) and similar interparticle spacings (∼20 nm). By decoupling the effects of interparticle magnetism, we identify and discuss the nanoparticles' magnetism in the context of their cation distributions. For example, an observed increase in the saturation magnetization of $CoFe_2O_4$ nanoparticles (∼2%) and $NiFe_2O_4$ nanoparticles (∼10%), and a decrease of the saturation magnetization of the $MnFe_2O_4$ nanoparticles (∼20%), all compared to their bulk counterparts is understood in terms of the nanoparticles' stoichiometries identified by low temperature Mössbauer spectroscopy in addition to a negligible number of Fe-ions distributed on the surface of all the particles, in keeping with the 20 nm nanoparticles surface-to-volume ratios.

2. Experimental methods

The nanoparticles were prepared using a method modified from the conventional organic phase process [19]. For the synthesis of $CoFe_2O_4$ nanoparticles, cobalt (II) acetate tetrahydrate (1 mmol) (⩾98.0%, Sigma-Aldrich) and iron (III) acetylacetonate (2 mmol) (97%, Sigma-Aldrich) were mixed with oleic acid (4 mL) (90%, Aldrich), oleylamine (4 mL) (70%, Aldrich) and dibenzyl ether (20 mL) (⩾98.0%, Sigma-Aldrich). The final mixture was sealed in a stainless-steel autoclave. The resulting solution was then heated to 200 °C and maintained at this temperature for 6 h under vigorous stirring. After removing the heat source, the autoclave was cooled to room temperature, and the black precipitate was washed several times with methanol to remove excess ligands. The black precipitate was then collected using a magnet and washed with chloroform. $MnFe_2O_4$ and $NiFe_2O_4$ nanoparticles were synthesized using a similar process, with manganese (II) acetylacetonate (1 mmol) (Sigma-Aldrich), nickel (II) acetate tetrahydrate (1 mmol) (98.0%, Sigma-Aldrich) and iron (III) acetylacetonate (2 mmol) (97%, Sigma-Aldrich) as reactants under similar reaction conditions, but autoclaved for different times (1 h and 4 h, respectively).

X-ray powder diffraction (XRD) patterns were collected at room temperature on a zero background quartz slide with a rotating stage using a Bruker D8 DaVinci diffractometer and CuKα radiation. All the XRD patterns have been analyzed using the Rietveld refinement technique (FullProf program [20]). Transmission electron microscopy (TEM) images of the samples were collected using a FEI Talos F200X S/TEM microscope. For TEM grid preparation, the nanoparticles were dispersed in hexane and aliquotes were dropped onto a carbon-coated copper grid. A dynamic light-scattering (DLS) apparatus (Photocor) was used with a 25 mW Coherent solid state laser with $\lambda = 632$ nm to measure the hydrodynamic size of the particles and size distributions of dilutions of $CoFe_2O_4$ and $NiFe_2O_4$ nanoparticles suspended in chloroform, and $MnFe_2O_4$ nanoparticles suspended in hexanes at room temperature. Transmission Mössbauer spectra were collected at 30 K in a Cryo closed-cycle refrigeration system using a WissEl spectrometer in constant acceleration mode with a 10 GBq ^{57}Co **Rh** source. The source drive velocity was calibrated using a 6 μm thick α-Fe foil at room temperature. Magnetometry and susceptometry was performed using a Quantum Design magnetic properties measurement system (MPMS XL-5).

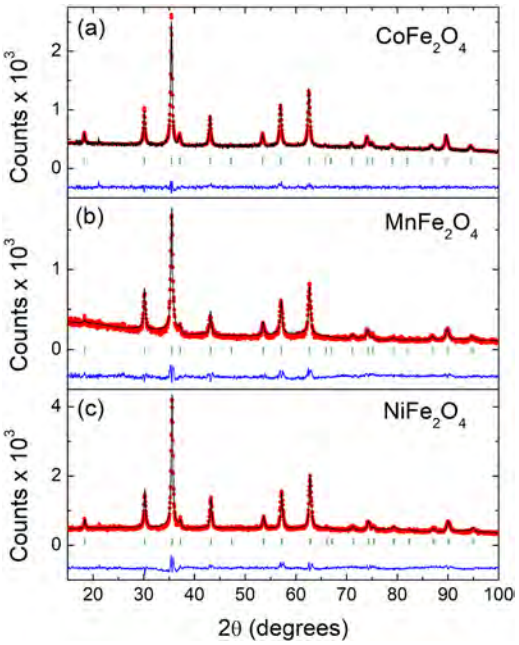

Figure 1. X-ray patterns of (a) $CoFe_2O_4$, (b) $MnFe_2O_4$, and (c) $NiFe_2O_4$ nanoparticles, with the results of the Rietveld refinements (black lines). The Bragg markers identify the reflections (green) and the residuals to the refinement are presented below (blue lines).

3. Results and discussion

3.1. Structural analysis

The x-ray diffraction patterns of $CoFe_2O_4$, $MnFe_2O_4$ and $NiFe_2O_4$ nanoparticles are shown in figures 1(a)–(c). All the reflections correspond to those of $CoFe_2O_4$, $MnFe_2O_4$ and $NiFe_2O_4$ nanoparticles and there is no evidence of any impurity. Refinements of the x-ray diffraction patterns using the FullProf program [20] revealed that each of the nanoparticle system have a spinel structure described by the cubic F $d\bar{3}$ m space group with lattice parameters 8.398 ± 0.001 Å for

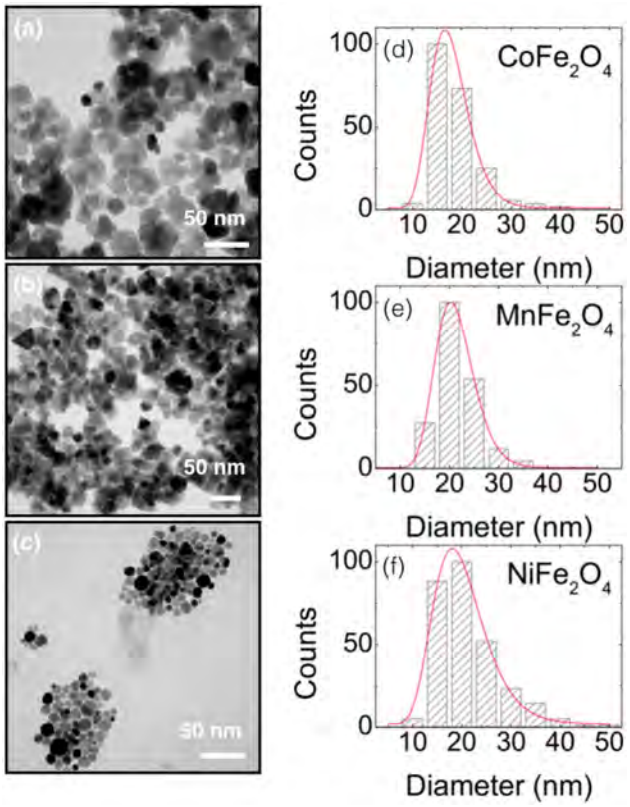

Figure 2. Typical TEM images of (a) $CoFe_2O_4$, (b) $MnFe_2O_4$, and (c) $NiFe_2O_4$ nanoparticles. The corresponding size histograms ((d)–(f)) are shown with log-normal fits (red lines).

$CoFe_2O_4$, 8.383 ± 0.001 Å for $MnFe_2O_4$, and 8.368 ± 0.001 Å for $NiFe_2O_4$. Scherrer broadening of the diffraction peaks incorporated into the refinements provides an estimate of ∼20 nm for the particle diameter of each of the ferrite nanoparticle systems.

Typical TEM images and the corresponding histogram plots of the sizes using ImageJ analysis [21] identify the particle size distribution of $CoFe_2O_4$, $MnFe_2O_4$ and $NiFe_2O_4$ nanoparticles are shown in figures 2(a)–(f). While $CoFe_2O_4$ and $NiFe_2O_4$ nanoparticles are nearly spherical, the $MnFe_2O_4$ nanoparticles present a mixed spherical and cubic morphology. The log-normal fits of the size histograms yielded the average diameters ($\langle D \rangle$) with standard deviations (σ) as $\langle D \rangle = 17 \pm 0.2$ nm and $\sigma = 0.22$ for $CoFe_2O_4$, $\langle D \rangle = 21 \pm 0.1$ nm and $\sigma = 0.19$ for $MnFe_2O_4$, $\langle D \rangle = 19 \pm 0.3$ nm and $\sigma = 0.27$ for $NiFe_2O_4$ nanoparticles. These sizes are in good agreement with those from the XRD refinements. We did not observe any peak asymmetry or unusual enhancement of the peak intensities in the XRD patterns of the ferrite systems which signifies the absence of any dominant or preferred crystallographic planes.

To better identify the clustering (that may impact the magnetism through interparticle interactions) and its relevant size scale, hinted at in the TEM images (e.g. figure 2(c)), DLS measurements were made on nanoparticles suspended in organics and analyzed with the DynaLS© software (figures 3(a)–(c)). The different size distributions with scattering angle, θ, indicate particle clusters in a size range ∼450–800 nm for $CoFe_2O_4$, ∼60–300 nm for $MnFe_2O_4$ and ∼400–750 nm for

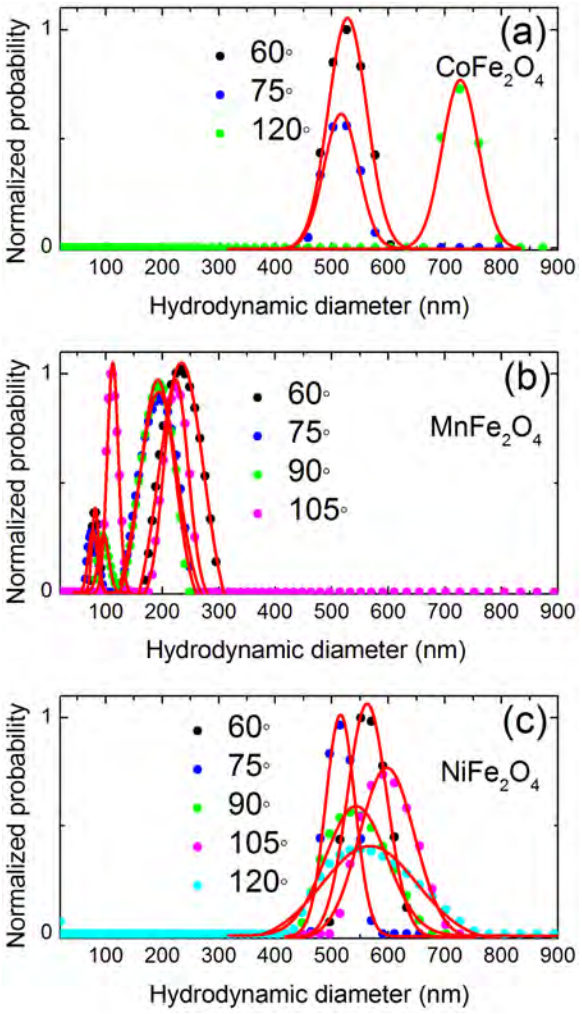

Figure 3. The hydrodynamic size distribution of (a) $CoFe_2O_4$, (b) $MnFe_2O_4$, and (c) $NiFe_2O_4$ nanoparticles measured by DLS. The red lines through the data at different scattering angles present the Gaussian fitting.

$NiFe_2O_4$ nanoparticles. Keep in mind that the DLS measurments identify a hydrodynamic size which reflects the oleic acid (OA) coatings in addition to possible clustering effects in suspension. Gaussian hydrodynamic particle size distributions with an average of $\sim 600 \pm 30$ nm for $CoFe_2O_4$, $\sim 150 \pm 20$ nm for $MnFe_2O_4$ and $\sim 550 \pm 50$ nm for $NiFe_2O_4$ nanoparticles are consistent with the values previously reported for different magnetic nanoparticles with surface coating [22], and indicates the existence of particle clusters of nanoparticles when in suspension.

To identify the compositions of the nanoparticles, Mössbauer spectra were collected at low temperature (30 K, well below the blocking temperature, T_B, to ensure the spin dynamics were negligible), as shown in figures 4(a)–(c). The spectra were fitted using a nonlinear least squares program with Lorentzian lineshapes, and the relative areas were used to determine the number of the ions in the sites. Excellent fits were obtained with superpositions of three subspectra for all samples. The Mössbauer parameters resulting from the fitting for each sample are listed in table 1. The presense of a $B2$ site is indicative of Fe ions that have a 2^+ charge [23], which

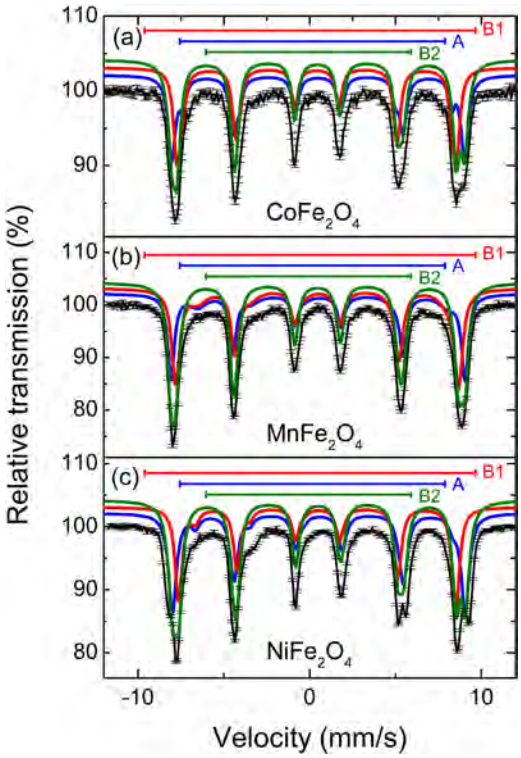

Figure 4. Mössbauer spectroscopy of (a) $CoFe_2O_4$, (b) $MnFe_2O_4$, and (c) $NiFe_2O_4$ nanoparticles at 30 K. The black points represent the experimental data and coloured lines through the data are the fits for the respective sites as described in the text.

Table 1. Mössbauer parameters obtained from the fitting: hyperfine field (B_{hf}), isomer shift (δ), linewidth (Γ), and area ratio of the A and B site components.

$CoFe_2O_4$				
	B_{hf} (T)	δ (mm s^{-1})	Γ (mm s^{-1})	Area (%)
A	50.4 ± 0.1	0.40 ± 0.01	0.23 ± 0.02	45.7 ± 4.2
B1	52.9 ± 0.1	0.49 ± 0.01	0.26 ± 0.01	45.6 ± 3.6
B2	48.0 ± 0.3	0.50 ± 0.03	0.24 ± 0.05	8.7 ± 3.6
$MnFe_2O_4$				
	B_{hf} (T)	δ (mm s^{-1})	Γ (mm s^{-1})	Area (%)
A	50.9 ± 0.1	0.43 ± 0.01	0.27 ± 0.02	42.9 ± 6.5
B1	53.3 ± 0.1	0.48 ± 0.05	0.25 ± 0.01	49.6 ± 5.1
B2	45.0 ± 0.3	0.84 ± 0.03	0.29 ± 0.06	7.5 ± 2.4
$NiFe_2O_4$				
	B_{hf} (T)	δ (mm s^{-1})	Γ (mm s^{-1})	Area (%)
A	50.2 ± 0.1	0.45 ± 0.01	0.24 ± 0.01	42.4 ± 5.1
B1	53.0 ± 0.1	0.53 ± 0.01	0.28 ± 0.01	51.1 ± 4.6
B2	46.6 ± 0.2	0.85 ± 0.04	0.28 ± 0.05	6.5 ± 3.4

is likely due to some B-sites residing on the surface of the crystallites. However, unlike the Mössbauer spectra of many nanoscale ferrites [24, 25], no electric field gradient on the Fe-ions (i.e. a doublet) was observed which is expected for significant broken coordination. Estimate of the surface spin to core spin population ratio of ∼0.1 for all samples was calculated using the relative ratio of sublattices from Mössbauer measurements. This value of the ratio of surface to core spin is exactly matching with the value of ∼0.1 was obtained for all samples by considering the surface layer thickness of order of the lattice parameter [26, 27] according to chemical core-shell model [28]. These results indicated that there is a negligible number of Fe-ions distributed on the surface of all the particles. A study of size dependent magnetic properties of manganese ferrite fine particles revealed that the surface effects disappear when the particle size is larger than ∼20 nm and our particles are in the same size range [29].

B_{hf} represents the hyperfine field that is proportional to the interaction between the Fe nucleus and its surrounding magnetic field, δ represents the isomer shift that is responsible for interaction occuring between the nucleus and the s-electrons (density), and Γ is the FWHM Lorentzian linewidth (0.133 ± 0.003 mm s^{-1} is the source's linewidth that is a measure of the lifetime of the excited state of the nucleus), and the spectral area is directly proportional to the number of Fe atoms in the A and B sites, respectively. The sextet with the smallest isomer shift is assigned to the Fe^{+3} ions occupying the tetrahedral sites. Because the number of d-electrons in the Fe^{+2} ions is larger than Fe^{+3} ions, the nucleus becomes more strongly shielded from s-electrons [30], the larger isomer shift is assigned to Fe^{+2} ions occupying the octahedral sites. The third sextet with the smallest hyperfine field interpreted as the presence of ∼9% Fe^{2+} ions for $CoFe_2O_4$, ∼8% Fe^{2+} ions for $MnFe_2O_4$ and ∼7% Fe^{2+} ions for $NiFe_2O_4$ nanoparticles occupying on the surface of the nanoparticles [31]. In addition, the Γs of the individual sites reflect the local site disorder, as expected from nanoparticles and in agreement with the local stress and strain, for example, mirrored in the Scherrer-broadened x-ray diffraction pattern reflections.

The distributions of the cations in tetrahedral and octahedral sites obtained from the Mössbauer fits lead to a chemical formula of $(Co^{2+}_{0.02}Fe^{3+}_{1.00})\,[Co^{2+}_{0.81}Fe^{3+}_{0.99}Fe^{2+}_{0.19}]O_4^{-2}$ for Co-ferrite, $(Mn^{2+}_{0.26}Fe^{3+}_{0.86})\,[Mn^{2+}_{0.80}Fe^{3+}_{1.00}Fe^{2+}_{0.15}]O_4^{-2}$ for Mn-ferrite and $(Ni^{2+}_{0.36}Fe^{3+}_{0.83})\,[Ni^{2+}_{0.78}Fe^{3+}_{1.00}Fe^{2+}_{0.13}]O_4^{-2}$ for Ni-ferrite nanoparticles. Mössbauer spectroscopy is a direct measure of the Fe ion environments [17] so the numbers of Co, Mn and Ni ions in the systems were estimated from charge balance arguments. Thus, the degree of inversion, x, was determined from the fraction of Co, Mn and Ni ions occupied in octahedral sites corresponded to that ∼98% of Co^{+2} ions, ∼80% of Mn^{+2} ions and ∼80% of Ni^{+2} ions in octahedral sites. These results indicated that the each of samples has a partially inverted (mixed) structure of a spinel ($0 < x < 1$) with high degree of inversion. All our values are comparable with previous reports [8, 31, 32].

3.2. Magnetic analysis

In order to study the magnetism of nanoparticles, the same amount of dried nanoparticles and GE varnish (VGE 7031) were mixed to keep the particles stabilized with the similar interparticle spacings. The interparticle spacings, $\langle d \rangle$, were estimated assuming a distribution of spherical particles via $\langle d \rangle = \frac{\langle D \rangle}{2}\left(\frac{4\pi}{3\chi_v}\right)$, where $\langle D \rangle$ is the mean nanoparticle diameter (estimated from XRD and TEM observations) and χ_v is the volume fraction of the nanoparticles. The interparticle

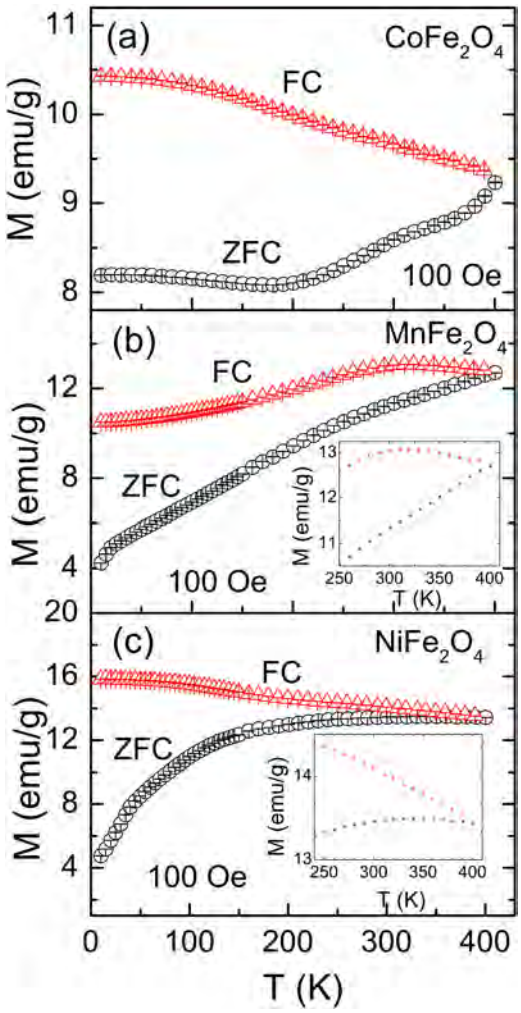

Figure 5. Temperature dependence of the ZFC and FC magnetization of (a) $CoFe_2O_4$, (b) $MnFe_2O_4$, and (c) $NiFe_2O_4$ nanoparticles. The insets show the high temperature regions.

spacings were $\langle d\rangle = 20$ nm, $\langle d\rangle = 25$ nm, $\langle d\rangle = 24$ nm for $CoFe_2O_4$, $MnFe_2O_4$ and $NiFe_2O_4$ nanoparticles, respectively.

The zero-field cooled (ZFC) and field-cooled (FC) low-field magnetization temperature-dependence (M-T) of the $CoFe_2O_4$, $MnFe_2O_4$ and $NiFe_2O_4$ nanoparticles were measured with an applied field of 100 Oe in the temperature range of 10–400 K for each sample, as shown in figures 5(a)–(c). For the ZFC measurements, the samples were first cooled down to 10 K at zero-field and then the magnetization was measured up to 400 K at a field of 100 Oe. In the FC sequence, the data were collected in the cooling cycle using the same magnetic field. In a ZFC-FC M-T scan of nanoparticles undergoing dynamical freezing that experience both inter- and intraparticle effects on the magnetism, three characteristic properties can often be distinguished [33]. The blocking temperature (T_B) where the maximum of the ZFC magnetization, the irreversibility temperature (T_{irr}) where the ZFC magnetization departs from the FC one due to interparticle interactions and $f(V)$, the particle size distribution from the $\mathrm{d}(M_{FC} - M_{ZFC})/\mathrm{d}T$ versus T shape.

In a ZFC measurement, M_{ZFC} increases at first with warming and then reaches the maximum value at T_B. At $T < T_B$ the particles are called in blocked regime as their magnetic moments directions are fixed along the applied field. At $T > T_B$, M_{ZFC} begins to decrease with increasing temperature and the particles are called in superparamagnetic regime in which single-domain moments fluctuate about their easy axis [34]. As can be seen from figures 5(a)–(c), $T_B > 400$ K for the $CoFe_2O_4$, $MnFe_2O_4$ and $NiFe_2O_4$ nanoparticles.

The broadening of the M_{ZFC} of $NiFe_2O_4$ nanoparticles is due to the wide particle size distribution and/or interparticle interactions [35]. The presence of clusters in the $NiFe_2O_4$ nanoparticles can couple the magnetizations of the neighbouring particles with increasing correlation lengths and thus increase the T_B of these nanoparticles.

A maximum at T_{max} in the ZFC magnetization is related to blocking effects which is not observed in the ZFC magnetization of $CoFe_2O_4$ and $MnFe_2O_4$ nanoparticles, indicating that $NiFe_2O_4$ is having a lower average energy barrier than the $CoFe_2O_4$ and $MnFe_2O_4$ [8]. As shown in the figure 5(a), the temperature dependence of the magnetization of $CoFe_2O_4$ nanoparticles exhibit a cusp around ~320 K in the ZFC magnetization. It can be attributed to the freezing of particles with smaller size which can lead to spin-glass like phase formation [36]. Different from $CoFe_2O_4$ nanoparticles, the magnetization of $MnFe_2O_4$ and $NiFe_2O_4$ nanoparticles in ZFC with warming decreases below T_B and no saturation is observed even down to 10 K. It can be attributed to lower anisotropy energy barrier of $MnFe_2O_4$ and $NiFe_2O_4$ compared to $CoFe_2O_4$ nanoparticles. Below T_B, the decreasing characteristic of M_{ZFC} with warming is related to random orientation of magnetization along the easy axes at low temperatures without applied field due to anisotropy [37].

The magnetization in FC with cooling slightly increases as the temperature decreases down to ~100 K for $CoFe_2O_4$ and $NiFe_2O_4$ and ~320 K for $MnFe_2O_4$ nanoparticles. At the temperatures below ~100 K for $CoFe_2O_4$ and $NiFe_2O_4$, ~50 K for $MnFe_2O_4$ nanoparticles the magnetization in FC with cooling exhibits nearly flat characteristic which indicates the existence of interparticle interactions [37]. The observed cusp near ~310 K in the M_{FC} plot with cooling of $MnFe_2O_4$ nanoparticles is indicative of the presence of strong interparticle interactions which is in agreement with Monte Carlo simulations [38]. Similar behaviour has been reported for $MnFe_2O_4$ nanoparticles with mean crystallite size of ~2 nm and Co particles embedded in Mn matrix with ~5% volume fraction which have strong dipolar and long-range interparticle interactions, respectively [39]. The collective behaviour of particles through the strong interparticle interactions shows similarities with the spin-glass systems [40], such as the existence of a maximum in M_{FC} plot. Since the interparticle interaction energy is much larger than the individual particle anisotropy energy in the presence of strong interparticle interactions the magnetic properties of a system can be characterized by a collective blocking of the particle moments [39]. It is clearly seen from the behaviour of M_{ZFC} and M_{FC} plot, the magnetic properties of our particles are more likely due to non-negligible interparticle interactions with formation of some clusters.

To investigate the blocking process in our systems the difference in the $(M_{FC} - M_{ZFC})$ plots are plotted against the

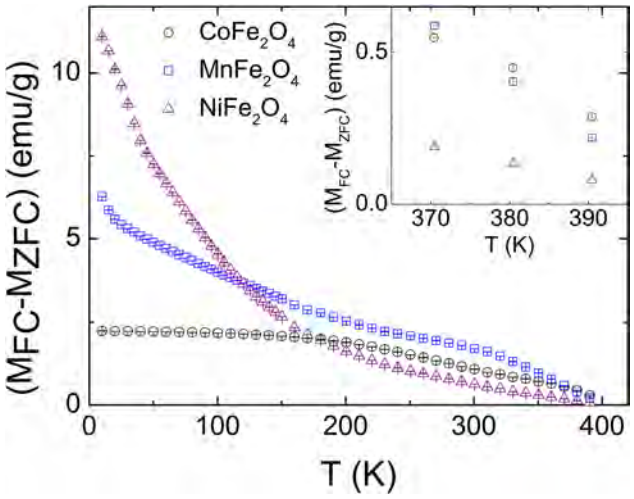

Figure 6. Temperature dependence of $(M_{FC} - M_{ZFC})$ of $CoFe_2O_4$ (○), $MnFe_2O_4$ (□), and $NiFe_2O_4$ (△) nanoparticles. The inset shows the high temperature region.

temperature as shown in figure 6. No clear coincidence of M_{ZFC} and M_{FC} was seen below ∼400 K for all samples as seen from the inset of figure 6. $NiFe_2O_4$ nanoparticles have larger irreversibility $(M_{FC} - M_{ZFC})$ which originates from the energy barriers of magnetic anisotropy [41], below ∼180 K compared to $CoFe_2O_4$ and $MnFe_2O_4$ nanoparticles. But at higher temperatures (above ∼180 K) the higher irreversibility of $CoFe_2O_4$ and $MnFe_2O_4$ compared to $NiFe_2O_4$ nanoparticles indicated that there are more amount of blocked particles in the samples [42] sign to a higher T_B for $CoFe_2O_4$ and $MnFe_2O_4$ compared to $NiFe_2O_4$ nanoparticles.

The field dependent magnetization of the nanoparticles were measured from 10 to 400 K under ±50 kOe applied fields. Typical hysteresis loops at 10 and 300 K are shown in figures 7(a)–(c). Hysteresis measurements indicated that $CoFe_2O_4$ nanoparticles become superparamagnetic with a blocking >400 K and higher than $MnFe_2O_4$ and $NiFe_2O_4$ with a blocking at ∼300 K with zero coercivity and remanance at these temperatures. The presence of small coercivities even at ∼400 K for $CoFe_2O_4$ show that the extra energy barrier arising from the interparticle interaction can inhibit spin flipping [43].

Saturation magnetization, $M_s(T)$ and the coercivity $(H_c(T))$ values of the nanoparticles were determined from the hysteresis loops by subtracting the diamagnetic contribution due to GE varnish, and known sample masses. $M_s(T)$, shown in figures 8(a)–(c) reflects the thermal behaviour of the nanoparticle's magnetization that is related to presence of spin waves, described by Bloch-like law [44] that incorporates finite size effects,

$$M(T) = M(0)[1 - BT^2] \quad (1)$$

where B is a spin-wave constant. Fitting $M_s(T)$ according to the equation (1) resulted in $M_s(0) = 95.18 \pm 0.33$ emu g^{-1} and $B = (1.46 \pm 0.03) \times 10^{-6}$ K^{-2} for $CoFe_2O_4$, $M_s(0) = 75.91 \pm 0.09$ emu g^{-1} and $B = (1.33 \pm 0.01) \times 10^{-6}$ K^{-2} for $MnFe_2O_4$, $M_s(0) = 69.93 \pm 0.03$ emu g^{-1} and $B = (1.27 \pm 0.01) \times 10^{-6}$ K^{-2} for $NiFe_2O_4$ nanoparticles.

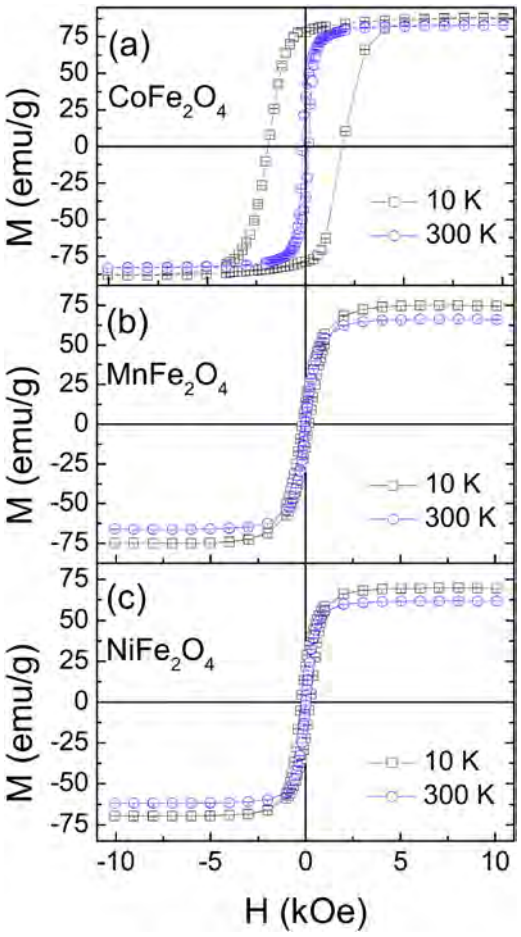

Figure 7. Hysteresis loops of (a) $CoFe_2O_4$, (b) $MnFe_2O_4$, and (c) $NiFe_2O_4$ at 10 (□) and 300 K (○).

The obtained values of B are comparable with values of ferrites reported previously [45]. $M_s(T)$ with T^2 dependence is an indication that there is an energy gap in the magnon fluctuation spectrum due to the finite-size effects [44]. $M_s(T)$ of the $CoFe_2O_4$ nanoparticles does not track well with equation (1); $M_s(T)$ ∼88 emu g^{-1} below ∼200 K. This behaviour may be explained by the magnetization of some of the bigger particles not rotating along with the magnetic field, causes a decrease in the magnetization at low temperatures. The saturation magnetization values are found to be $M_s(300\,K)$ ∼83 emu g^{-1} for $CoFe_2O_4$, ∼67 emu g^{-1} for $MnFe_2O_4$ and ∼62 emu g^{-1} for $NiFe_2O_4$. Considering a typical density of ∼5.3 g cm^{-3} [46] in the bulk forms of these ferrites, the $M_s(300\,K)$ values of the $CoFe_2O_4$, $MnFe_2O_4$ and $NiFe_2O_4$ are determined as 439.9, 355.1 and 328.6 emu cm^{-3}, respectively, which are comparable with values reported in [47].

These values represent a ∼20% decrease, and ∼2% and ∼10% increase compared to their bulk values at room temperature, for $CoFe_2O_4$, $MnFe_2O_4$ and $NiFe_2O_4$ respectively. M_s is governed by the distribution of cations in their respective sublattices [8, 48], and in nanoparticle systems, this is especially relevant as the nanoparticle core degree of inversion, x, and potential contribution of disordered spin structures from the surface (determined by the surface/volume ratio of the nanoparticles [48–50]) are competing effects.

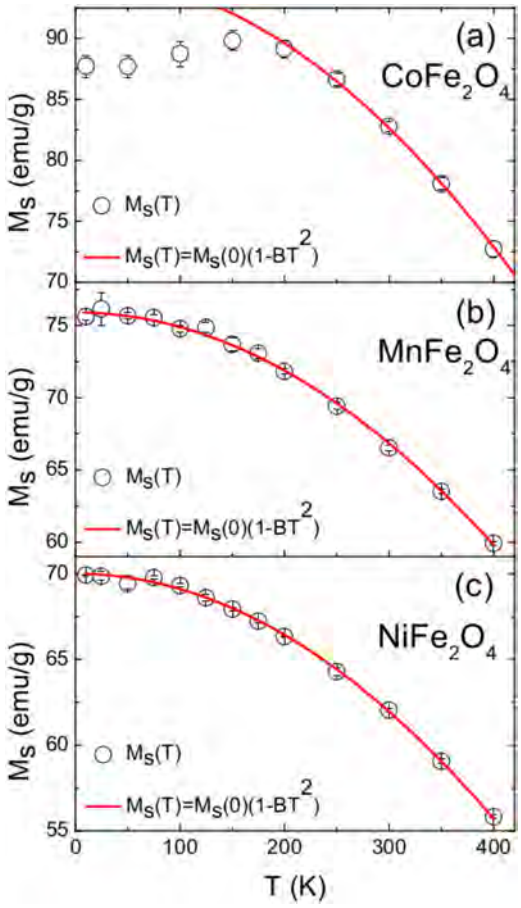

Figure 8. Temperature dependence of saturation magnetization (M_s) of (a) $CoFe_2O_4$, (b) $MnFe_2O_4$, and (c) $NiFe_2O_4$ nanoparticles. The red lines show the fits using equation (1).

To clarify these different effects on M_s, the contribution from the cation distributions to the magnetism via net magnetization per formula unit (n_{net}) were calculated using the Néel's sub-two-lattice model [51] with the relation, $n_{\text{net}} = M_B - M_A$, where M_B is the net magnetization of octahedral sites, and M_A is the net magnetization of tetrahedral sites in μ_B [52]. From the Mössbauer fit results the net magnetization per formula unit is found to be $3.04\mu_B$ for $CoFe_2O_4$, $4.00\mu_B$ for $MnFe_2O_4$ and $2.21\mu_B$ for $NiFe_2O_4$ nanoparticles. Generalizing that the net magnetization per unit formula of any ferrite with inverse spinel structure is simply the moment on the divalent ion which corresponds to values of magnetization of $3\mu_B$, $5\mu_B$ and $2\mu_B$ for $CoFe_2O_4$, $MnFe_2O_4$ and $NiFe_2O_4$ [6], one can clearly see that the calculated values of magnetization using Mössbauer spectra results are in good agreement with the observed ~20% decrease, and ~2% and ~10% increase of net magnetization compared to bulk for $CoFe_2O_4$, $MnFe_2O_4$ and $NiFe_2O_4$ nanoparticles. We conclude that migration of ~2% of Co^{2+} ions, ~25% of Mn^{2+} ions and ~32% of Ni^{2+} ions from octahedral sites to tetrahedral sites with the distribution of ~9%, ~8% and ~7% of Fe^{2+} ions on the surface are responsible for altered magnetization in $CoFe_2O_4$, $MnFe_2O_4$ and $NiFe_2O_4$ nanoparticles, respectively.

To characterize the magnetic anisotropy that is a measure of distribution of energy barriers in the system the

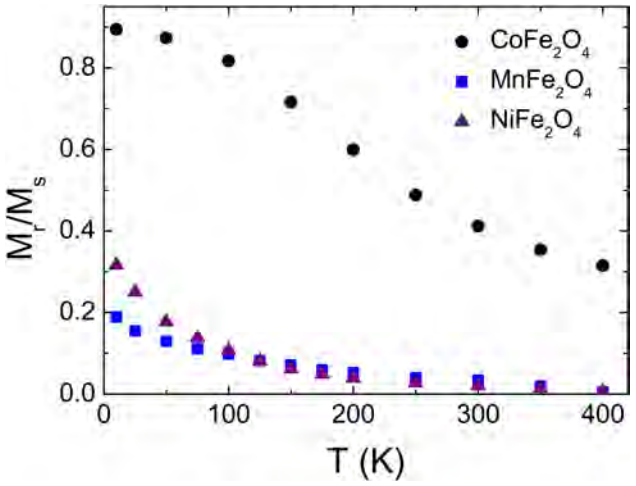

Figure 9. Squareness ratio, M_r/M_s as a function of temperature for the $CoFe_2O_4$ (●), $MnFe_2O_4$ (■), and $NiFe_2O_4$ nanoparticles (▲).

measurement of squareness (M_r/M_s) determined from the hysteresis measurements, is shown in figure 9. For randomly oriented particles with uniaxial anisotropy $M_r/M_s = 0.5$ is the expected (theoretical) value of the squareness at 0 K when nanoparticles are blocked [42]. The maximum squarenesses were found to be M_r/M_s (10 K) ~0.9, ~0.3, and ~0.2 for the $CoFe_2O_4$, $MnFe_2O_4$ and $NiFe_2O_4$ nanoparticles, respectively. The reduced (compared to 0.5) squarenesses of the $MnFe_2O_4$ and $NiFe_2O_4$ nanoparticles are in good agreement with previous studies [53] that indicated in general that the M_r/M_s of nanoparticulate systems will fall below the theoretical value—attributed to the frustration of the surface spins [53], noncoherent rotational magnetization processes, distribution of anisotropy fields and interparticle interactions [42]. $M_r/M_s > 0.5$ for the $CoFe_2O_4$ nanoparticles compared to theoretical maximum value (0.83–0.87) [54] of squareness indicates that the system is completely blocked with the tendency toward cubic magnetic anisotropy of particles [8, 49]. The cubic anisotropy of $CoFe_2O_4$ nanoparticles leads to a reduced energy barrier ($\Delta E(\mu_0 H) \approx KV/4$) to reversal compared to the uniaxial anisotropy systems ($\Delta E(\mu_0 H) \approx KV$) [55]. This will alter $H_c(T)$, as discussed below.

The coercive fields of the $CoFe_2O_4$, $MnFe_2O_4$ and $NiFe_2O_4$ nanoparticles at different temperatures determined from the hysteresis loops, are shown in figures 10(a)–(c). We observed that the coercivity increases with decreasing temperature for all samples. The coercivity versus temperature plots of the nanoparticles can be fitted using the following equation [56] by incorporating the temperature dependence of $M_s(T)$ from equation (1).

$$H_c(T) = \frac{2K}{M_s(T)}[1 - (T/T_B)^{1/2}]. \quad (2)$$

The fitted values of M(0) and B obtained from equation (1) were used to determine the values of K and T_B of the individual ferrite systems. From the fits, the K and T_B values were found to be $\sim(2.96 \pm 0.03) \times 10^6$ ergs cm^{-3} and 300 ± 1 K for the $CoFe_2O_4$ nanoparticles, $\sim(0.07 \pm 0.01) \times 10^6$ ergs cm^{-3} and 90 ± 3 K for the $NiFe_2O_4$ nanoparticles,

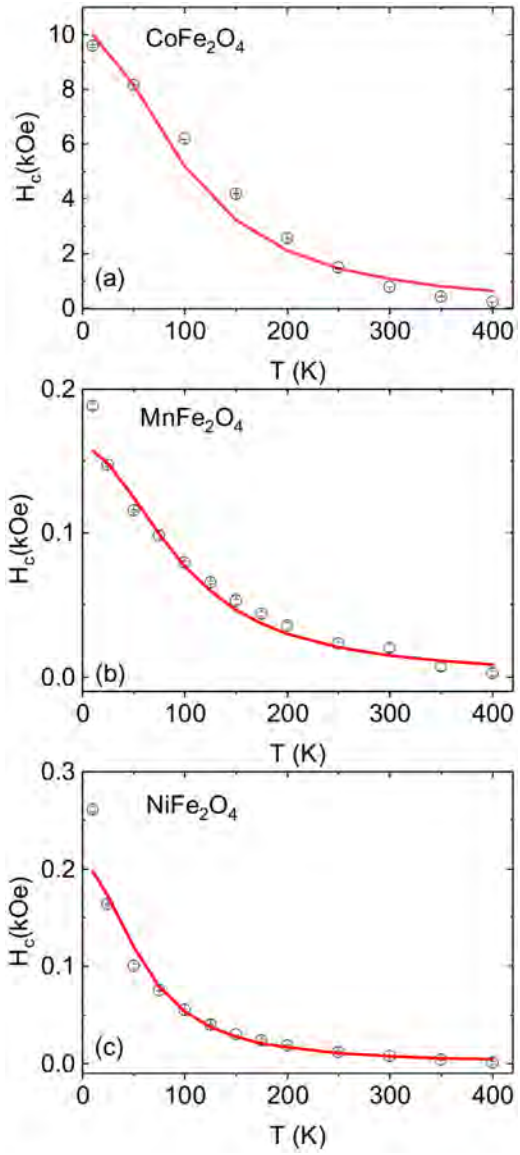

Figure 10. Temperature dependence of the coercivity for (a) $CoFe_2O_4$, (b) $MnFe_2O_4$, and (c) $NiFe_2O_4$ nanoparticles. The red lines show the fit according to equation (2) in the text.

and $\sim(0.04 \pm 0.01) \times 10^6$ ergs cm^{-3} and 210 ± 6 K for the $MnFe_2O_4$ nanoparticles. According to the T_B values from the fits of the temperature dependence of coercivity, it is expected that when the temperature is ~300 K for $CoFe_2O_4$, ~210 K for $MnFe_2O_4$ and ~90 K for $NiFe_2O_4$ nanoparticles, the energy barrier would be overcome by the thermal energy, and the coercivity will be zero if neglecting the interparticle interactions. These estimated values of T_B are lower than estimated from ZFC-FC measurements for all samples. The anisotropy constants determined from the fit of temperature dependence coercivity are found to be comparable with the bulk values [57, 58] for $CoFe_2O_4$ and $NiFe_2O_4$ nanoparticles, but higher (almost twice) for $MnFe_2O_4$ nanoparticles [59].

The 300 K H_c values for the $CoFe_2O_4$, $MnFe_2O_4$ and $NiFe_2O_4$ nanoparticles were found to be ~0.78 kOe, ~0.02 kOe and ~0.01 kOe, respectively. The H_c of $CoFe_2O_4$ nanoparticles is found to be in the range of bulk coercivity (~0.75–0.98 kOe) [60]. The H_c of $MnFe_2O_4$ nanoparticles has been found to be higher, while the $NiFe_2O_4$ nanoparticles has a lower one compared to bulk values [61, 62]. In general, nanoparticles are expected to have a smaller H_c than the bulk (~100 nm or smaller are single domain particles) [60]. But the observation of a wide range of coercivity of any material can be related to magnetic anisotropy, defects, strain, nature of the surface, interface, interparticle interactions [60], difference in the composition and grain size of the sample [63]. The obtained values of coercivities are consistent with the value of effective magnetic anisotropies determined from the temperature dependence of coercivity for $MnFe_2O_4$ and $NiFe_2O_4$ nanoparticles. One can clearly see from the description of the anisotropy field with cubic symmetry crystals [64] that a decrease and an increase of saturation magnetization compared to bulk counterparts due to cation distributions (as shown before) for $MnFe_2O_4$ and $NiFe_2O_4$ nanoparticles lead to an increase and a decrease of coercivities of particles, respectively. We concluded from this that the H_c values of the $MnFe_2O_4$ and $NiFe_2O_4$ nanoparticles are solely due to their effective magnetic anisotropies that reflect their intrinsic magnetic hardness [65].

4. Summary and conclusion

Nanoparticles of $CoFe_2O_4$, $MnFe_2O_4$ and $NiFe_2O_4$ with comparable sizes (~20 nm) and interparticle spacings (~20 nm) were synthesized using a method modified from the conventional organic phase process. The cation distributions of tetrahedral and octaheral sites of the particles were determined by Mössbauer spectroscopy. We found a high degree of inversion of ~0.98 for $CoFe_2O_4$, ~0.80 for $MnFe_2O_4$ and $NiFe_2O_4$ nanoparticles. The excellent fits of the Mössbauer spectra with more than two sextets are attributed to the presence of surface spins. We estimated a negligible surface to core spin population ratio of ~0.1 for all samples using Mössbauer results. A broadening of the M_{ZFC} plot with warming of $NiFe_2O_4$ nanoparticles is attributed to wide particle size distribution and/or interparticle interactions in the system. A small cusp around ~320 K in ZFC magnetization with warming of $CoFe_2O_4$ nanoparticles indicated spin-glass like phase formation. The non-negligible interparticle interactions for all samples are clearly reflected in ZFC-FC measurements of the particles. No clear coincidence of M_{ZFC} and M_{FC} was seen below ~400 K for all samples. Hysteresis measurements indicated that $CoFe_2O_4$ nanoparticles become superparamagnetic with a blocking >400 K and higher than $MnFe_2O_4$ and $NiFe_2O_4$ with a blocking at ~300 K. The magnetization at room temperature increases by ~2% for $CoFe_2O_4$, ~10% for $NiFe_2O_4$, but decreases by ~20% for $MnFe_2O_4$ nanoparticles compared to their bulk counterparts. An increasing behaviour of coercive field with decreasing temperature interpreted as thermal activation of the particle moments are due to anisotropy barrier according to equation (2). The effective magnetic anisotropies of the particles estimated from temperature dependence of coercivity were found to be comparable to bulk counterparts. The consistency between the effective magnetic

anisotropy and coercivity of $MnFe_2O_4$ and $NiFe_2O_4$ indicated that the coercivity of the particles is due to effective magnetic anisotropy which is the intrinsic hardness of the system. But the inconsistency between the effective magnetic anisotropy and coercivity of $CoFe_2O_4$ nanoparticles indicated that the anisotropy of the system may be governed by extrinsic factors. A comparison between three typical ferrite systems with comparable sizes and comparable interparticle spacings is useful to understand the effect of distribution of cations in tetrahedral and octahedral sites on the overall magnetism.

Acknowledgments

The authors thank the Scientific and Technological Research Council of Turkey (TUBITAK) and Natural Sciences and Engineering Research Council of Canada (NSERC). This paper has been granted by the Muğla Sıtkı Koçman University Scientific Research Project Coordination through Project Grant Number: (14/066).

ORCID iDs

Ç E Demirci https://orcid.org/0000-0002-3081-0691

References

[1] Tomar M, Singh S, Perales-Perez O, Guzman R, Calderon E and Rinaldi-Ramos C 2005 *Microelectron. J.* **36** 475–9
[2] McMichael R, Shull R, Swartzendruber L, Bennett L and Watson R 1992 *J. Magn. Magn. Mater.* **111** 29–33
[3] Poddar P, Gass J, Rebar D, Srinath S, Srikanth H, Morrison S and Carpenter E 2006 *J. Magn. Magn. Mater.* **307** 227–31
[4] Yang H, Zhang C, Shi X, Hu H, Du X, Fang Y, Ma Y, Wu H and Yang S 2010 *Biomaterials* **31** 3667–73
[5] Sharifi I, Shokrollahi H and Amiri S 2012 *J. Magn. Magn. Mater.* **324** 903–15
[6] Cullity B D and Graham C D 2011 *Introduction to Magnetic Materials* (New York: Wiley)
[7] Sickafus K E, Wills J M and Grimes N W 1999 *J. Am. Ceram. Soc.* **82** 3279–92
[8] Carta D, Casula M F, Falqui A, Loche D, Mountjoy G, Sangregorio C and Corrias A 2009 *J. Phys. Chem.* C **113** 8606–15
[9] Gyergyek S, Makovec D, Kodre A, Arčon I, Jagodič M and Drofenik M 2010 *J. Nanoparticle Res.* **12** 1263–73
[10] Nlebedim I, Melikhov Y and Jiles D C 2014 *J. Appl. Phys.* **115** 043903
[11] Ranvah N, Nlebedim I, Melikhov Y, Snyder J, Williams P, Moses A and Jiles D 2009 *IEEE Trans. Magn.* **45** 4261–4
[12] Jovic N G, Masadeh A S, Kremenovic A S, Antic B V, Blanusa J L, Cvjeticanin N D, Goya G F, Antisari M V and Bozin E S 2009 *J. Phys. Chem.* C **113** 20559–67
[13] Rath C, Anand S, Das R, Sahu K, Kulkarni S, Date S and Mishra N 2002 *J. Appl. Phys.* **91** 2211–5
[14] Wang J, Wu Y and Zhu Y 2007 *Int. J. Mod. Phys.* B **21** 723–9
[15] Vaingankar A, Khasbardar B and Patil R 1980 *J. Phys. F: Met. Phys.* **10** 1615
[16] Chen J, Sorensen C, Klabunde K, Hadjipanayis G, Devlin E and Kostikas A 1996 *Phys. Rev.* B **54** 9288
[17] Sawatzky G, Van Der Woude F and Morrish A 1969 *Phys. Rev.* **187** 747
[18] Willard M A, Nakamura Y, Laughlin D E and McHenry M E 1999 *J. Am. Ceram. Soc.* **82** 3342–6
[19] Sun S, Zeng H, Robinson D B, Raoux S, Rice P M, Wang S X and Li G 2004 *J. Am. Chem. Soc.* **126** 273–9
[20] Rodríguez-Carvajal J 1993 *Physica* B **192** 55–69
[21] Schneider C A, Rasband W S and Eliceiri K W 2012 *Nat. Methods* **9** 671–5
[22] Lim J, Yeap S P, Che H X and Low S C 2013 *Nanoscale Res. Lett.* **8** 381
[23] Persoons R, De Grave E, De Bakker P and Vandenberghe R 1993 *Phys. Rev.* B **47** 5894
[24] Grigorova M, Blythe H, Blaskov V, Rusanov V, Petkov V, Masheva V, Nihtianova D, Martinez L M, Munoz J and Mikhov M 1998 *J. Magn. Magn. Mater.* **183** 163–72
[25] Šepelák V, Baabe D, Mienert D, Schultze D, Krumeich F, Litterst F and Becker K 2003 *J. Magn. Magn. Mater.* **257** 377–86
[26] Gomes J, Azevedo G, Depeyrot J, Mestnik-Filho J, Paula F, Tourinho F and Perzynski R 2012 *J. Phys. Chem.* C **116** 24281–91
[27] Ferreira L, Cruz M, Oliveira M, Mendo S, Alves A, Godinho M and Carvalho M 2016 *RSC Adv.* **6** 73506–16
[28] Gomes J D A, Sousa M H, Tourinho F A, Aquino R, da Silva G J, Depeyrot J, Dubois E and Perzynski R 2008 *J. Phys. Chem.* C **112** 6220–7
[29] Tang Z, Sorensen C, Klabunde K and Hadjipanayis G 1991 *J. Appl. Phys.* **69** 5279–81
[30] Walker L, Wertheim G K and Jaccarino V 1961 *Phys. Rev. Lett.* **6** 98
[31] Chinnasamy C, Narayanasamy A, Ponpandian N, Chattopadhyay K, Shinoda K, Jeyadevan B, Tohji K, Nakatsuka K, Furubayashi T and Nakatani I 2001 *Phys. Rev.* B **63** 184108
[32] Atif M, Nadeem M and Siddique M 2015 *Appl. Phys.* A **120** 571–8
[33] Knobel M, Nunes W, Socolovsky L, De Biasi E, Vargas J and Denardin J C 2008 *J. Nanosci. Nanotechnol.* **8** 2836–57
[34] Van Lierop J and Ryan D 2000 *Phys. Rev. Lett.* **85** 3021
[35] Mitra S, Mandal K and Kumar P A 2006 *J. Magn. Magn. Mater.* **306** 254–9
[36] Singh M K, Prellier W, Singh M, Katiyar R S and Scott J 2008 *Phys. Rev.* B **77** 144403
[37] Sharma S, Kumar R, Kumar S, Knobel M, Meneses C, Kumar V S, Reddy V, Singh M and Lee C 2008 *J. Phys.: Condens. Matter* **20** 235214
[38] Chantrell R, Coverdale G, El Hilo M and O'Grady K 1996 *J. Magn. Magn. Mater.* **157** 250–5
[39] Fiorani D and Peddis D 2014 *J. Phys.: Conf. Ser.* **521** 012006
[40] Peddis D, Cannas C, Musinu A and Piccaluga G 2008 *J. Phys. Chem.* C **112** 5141–7
[41] Hyeon T, Chung Y, Park J, Lee S S, Kim Y W and Park B H 2002 *J. Phys. Chem.* B **106** 6831–3
[42] Batlle X, Garcia del Muro M, Tejada J, Pfeiffer H, Görnert P and Sinn E 1993 *J. Appl. Phys.* **74** 3333–40
[43] Zhang Y, Liu Y, Fei C, Yang Z, Lu Z, Xiong R, Yin D and Shi J 2010 *J. Appl. Phys.* **108** 084312
[44] Hendriksen P V, Linderoth S and Lindgård P A 1993 *Phys. Rev.* B **48** 7259
[45] Chandekar K V and Kant K M 2017 *Adv. Mater. Lett.* **8** 435–43
[46] Thang P D, Rijnders G and Blank D H 2005 *J. Magn. Magn. Mater.* **295** 251–6
[47] Blaskov V, Petkov V, Rusanov V, Martinez L M, Martinez B, Munoz J and Mikhov M 1996 *J. Magn. Magn. Mater.* **162** 331–7
[48] Virumbrales-del Olmo M, Delgado-Cabello A, Andrada-Chacón A, Sánchez-Benítez J, Urones-Garrote E, Blanco-Gutiérrez V, Torralvo M and Sáez-Puche R 2017 *Phys. Chem. Chem. Phys.* **19** 8363–72

[49] Peddis D, Orrù F, Ardu A, Cannas C, Musinu A and Piccaluga G 2012 *Chem. Mater.* **24** 1062–71
[50] Peddis D, Mansilla M V, Mørup S, Cannas C, Musinu A, Piccaluga G, D'Orazio F, Lucari F and Fiorani D 2008 *J. Phys. Chem.* B **112** 8507–13
[51] Neel L 1948 *Ann. Phys* **3** 137–98
[52] Lohar K, Pachpinde A, Langade M, Kadam R and Shirsath S E 2014 *J. Alloys Compd.* **604** 204–10
[53] Vestal C R, Song Q and Zhang Z J 2004 *J. Phys. Chem.* B **108** 18222–7
[54] Soares J, Galdino V and Machado F 2014 *J. Magn. Magn. Mater.* **350** 69–72
[55] Virden A, Wells S and O'Grady K 2007 *J. Magn. Magn. Mater.* **316** e768–71
[56] Shendruk T, Desautels R, Southern B and Van Lierop J 2007 *Nanotechnology* **18** 455704
[57] Carvalho M, Lima R, Meneses C, Folly W, Sarmento V, Coelho A and Duque J 2016 *J. Appl. Phys.* **119** 093909
[58] Du Y, Xu M, Wu J, Shi Y, Lu H and Xue R 1991 *J. Appl. Phys.* **70** 5903–5
[59] Yoon S and Krishnan K M 2011 *J. Appl. Phys.* **109** 07B534
[60] Limaye M V, Singh S B, Date S K, Kothari D, Reddy V R, Gupta A, Sathe V, Choudhary R J and Kulkarni S K 2009 *J. Phys. Chem.* B **113** 9070–6
[61] Aslibeiki B, Kameli P and Ehsani M 2016 *Ceram. Int.* **42** 12789–95
[62] Shan A, Wu X, Lu J, Chen C and Wang R 2015 *CrystEngComm* **17** 1603–8
[63] Chinnasamy C, Jeyadevan B, Shinoda K, Tohji K, Djayaprawira D, Takahashi M, Joseyphus R J and Narayanasamy A 2003 *Appl. Phys. Lett.* **83** 2862–4
[64] Gubin S P, Koksharov Y A, Khomutov G and Yurkov G Y 2005 *Russ. Chem. Rev.* **74** 489–520
[65] Blanco-Gutiérrez V, Gallastegui J, Bonville P, Torralvo-Fernández M J and Sáez-Puche R 2012 *J. Phys. Chem.* C **116** 24331–9